Journal of Materials Chemistry A

Accepted Manuscript

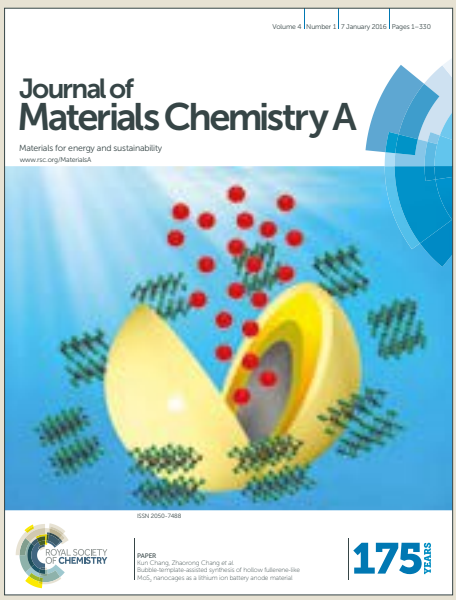

ROYAL SOCIETY OF CHEMISTRY

rsc.li/materials-a

View Article Online
DOI: 10.1039/C8TA04178D

Journal of Materials Chemistry A

ARTICLE

Two-Dimensional Cationic Covalent Organic Framework Membrane for Selective Molecular Sieving

Wenxiang Zhang,[ab] Liming Zhang,[a] Haifeng Zhao,[a] Bin Li*[a] and Heping Ma*[c]

Received 00th January 20xx,
Accepted 00th January 20xx

DOI: 10.1039/x0xx00000x

www.rsc.org/

The search of new-type membrane materials with ideal molecular sieving caused widely interest in both academia and industry. Covalent organic frameworks (COFs) are excellent candidates for efficient molecular separation because of their well-defined pore structure and fine-tuning pore size. However, existing synthetic approaches of COFs mainly result in insoluble and unprocessable powder, which severely restrict their widespread applicability. In this work, a facile bottom-up interfacial crystallization approach to obtain a two-dimensional (2D) cationic COF, EB-COF:Br nanosheets is reported. Then a layer-by-layer restacking process is performed to fabricate continuous and dense 2D ionic COF membrane with tunable thickness by simple vacuum filtration. The 2D COF membrane shows much higher solvent permeability than graphene-oxide membranes and commercial nanofiltration membranes because of their high porosity. Moreover, due to there are abundant positive charge sites in pore walls, the EB-COF:Br membrane demonstrates highly selective sieving performance for dye molecules/ions with different charges and sizes. The EB-COF:Br membrane can efficiently reject ~>98% of anionic dye molecules/ions, while maintaining high solvent permeability. The cationic 2D COF membrane far outperform other nanofiltration membranes in terms of excellent selective molecular/ionic sieving and superior solvent permeability. The result suggested that ionic COFs membrane can offer a new avenue for separation technology.

Introduction

Porous membranes with controllable pore size in nanometer are of interest for efficient and energy-saving separation processes.[1-6] Recently, the observation of precise molecular sieving and fast solvent permeation through graphene-oxide membranes (GOMs) has aroused intense interest due to their potential application in water filtration, molecular separation and desalination.[7-11] The laminar GOMs can be readily obtained through vacuum filtration, spin coating or a layer-by-layer self-assembly approach.[12-15] The selective molecular sieving of laminar GOMs is primarily dependent on size cut-off effect.[16-18] However, the pores of laminar GOMs—that is the interstitial space between graphene oxide laminates—are difficult to maintain when immersing laminar GOMs in aqueous solution due to the swell of interlayer channels (As schematically elucidated Fig. 1a).[19-21] The mass transport across the laminar GOMs in vertical direction is usually in low permeability because of the intricate transport path (Fig. 1a).[22,23] These challenges hinder the potential applications of laminar GOMs in real separation process.

Two-dimensional covalent organic frameworks (2D COFs) are emerging crystalline porous materials with precisely controlled pore size, functionalized pore surface and nano channel toward their vertical direction (Fig. 1b).[24-30] Most of the conventional COFs synthetic approaches offer poor control of their morphology and result in insoluble and unprocessable microcrystalline powder.[31-34] Although some COFs powder can be transformed into covalently organic nanosheets (CONs) via further exfoliated under mechanical grinding, ultra-sonication or chemical process,[35-42] the resulting CONs lead to tiny size and vast internal structural defects due to the rough operation procedure, which impedes CONs further assemble into integral and large-scale COFs membrane for separation.[43] Recently, Banerjee et.al reported the preparation of COFs thin films in virtue of interface crystallization process.[44] This strategy allows simultaneous control over crystallization and morphology of COF films. However, these COFs films still rely on neutral framework structures. Integration of ionic modules into porous membranes would induce novel functions distinct from those of neutral membranes, especially when the pores size of the membrane is below 100 nm.[45] In extremely limited space, the remarkable electrostatic interaction is superimposed with confinement of the nano channels; the mass transport in the charged channel will be double-controlled by size and charge.[46,47] In this sense, lots of unexpected and exciting phenomena of nano confined transports such as highly selective ion permeation and ultrafast solvent permeation are predictable in the charged COFs membrane.[48] Accordingly, we prepared a 2D cationic COF membrane with accessible ionic units and uniform nanosize channels for selective molecular sieving.

[a] State Key Laboratory of Luminescence and Applications, Changchun Institute of Optics, Fine Mechanics and Physics, Chinese Academy of Sciences, Changchun 130033, P. R. China. E-mail: libinteacher@163.com
[b] University of Chinese Academy of Sciences, Beijing 100039, P. R. China.
[c] School of Chemical Engineering and Technology, Xi'an Jiaotong University, Xi'an 710049, China. E-mail: maheping@mail.xjtu.edu.cn

† Electronic Supplementary Information (ESI) available: Experimental details, materials and reagents, apparatus, conditions and methods. See DOI: 10.1039/x0xx00000x

View Article Online
DOI: 10.1039/C8TA04178D

We introduced a salt-mediated technique to fabricate cationic COF, EB-COF:Br as large-scale membranes by combining a cationic monomer, ethidium bromide (EB) (3,8-diamino-5-ethyl-6-phenylphenanthridinium bromide), with 1,3,5-triformylphloroglucinol (TFP) through a Schiff base reaction under 35□ (Fig. 1c).[31,44] The highly crystalline porous 2D cationic COF nanosheets were definitely retained at the liquid-liquid interface and were easily transferable to various substrates (Fig. 1d and Fig. S1, ESI†).[44] Then a layer-by-layer restacking process was performed to assemble continuous and dense EB-COF:Br membrane with tunable thickness by handy vacuum filtration of different amounts of nanosheets dispersion liquid on the nylon 66 support (Fig. 1e).[49,50] The cationic EB-COF:Br membrane exhibited excellent selective sieving for ionic pollutants of different molecular sizes and charges, along with high solvent permeability. To the best of our knowledge, this is the first positively charged 2D COFs membrane with excellent selective sieving performance.

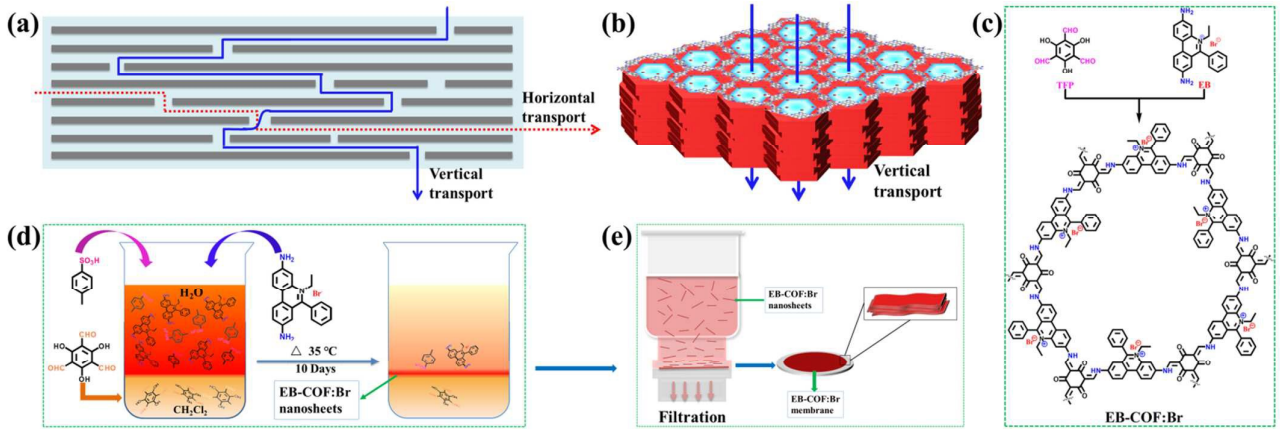

Fig. 1 (a) The model of lamellar film with massive arrays of 2D graphene oxide (GO) sheets, the mass transfer can be achieved in both along the sheets (horizontal transport) and across GO sheets at defects (vertical transport). (b) The mass transport across the COFs membrane along the 1D nano channels toward vertical direction. (c) Chemical structures schematic of the synthesis of EB-COF:Br via the condensation of EB and TFP under 35℃. (d) Schematic representation of the interfacial crystallization process used to synthesize the EB-COF:Br nanosheets, the bottom faint-yellow layer corresponds to aldehyde in dichloromethane solution, and the top orange-red layer is EB amine-PTSA aqueous solution. (e) Schematic representation of the preparation process of EB-COF:Br membrane via layer-by-layer restacking of EB-COF:Br nanosheets.

Results and discussion

The interfacial crystallization approach was used to synthesize stable keto-enol tautomerism-based EB-COF:Br nanosheets by a Schiff base reaction (Fig. 1c).[44,51-53] The Fourier transform infrared (FT-IR) spectra of initial monomers and EB-COF:Br had been measured and shown in Fig. S2a (ESI†). The aldehyde group stretching bands of TFP (-C=O at 1642 cm^{-1}, O=C-H at 2890 cm^{-1}) and the N-H stretching bands of EB are disappeared (3196 cm^{-1}, 3303 cm^{-1}), which provides a direct evidence for the completion of co-condensation reaction. Meanwhile, the lack of -OH and imine (C=N) stretches and the rise of the C=C stretching peak at 1594 cm^{-1} (Fig. S2b, ESI†) demonstrate that EB-COF:Br exists in the keto form.[54] One of the advantages of interfacial crystallization is we can transfer the film onto different substrates. Fig. 2a is the digital image of a large-scale film we transferred on porous glass. We further use atomic force microscopy (AFM), transmission electron microscope (TEM) and scanning electron microscopy (SEM) to gain insight into the internal structure of the COF nansheets and membrane. The AFM was used to estimate the thickness of the EB-COF:Br nanosheets. The nanosheets were dispersed into ethanol by sonication and then drop-casted on silicon wafer for AFM measurement. AFM analysis results indicates that the heights of EB-COF:Br nanosheets are in the range of ~155-165nm (Fig. 2d, e). These nanosheets were then loaded on carbon-coated copper grid for TEM analysis. As shown in Fig. 2g, the TEM image of EB-COF:Br nanosheets reveals a high degree of crystallinity, as demonstrated by the clear lattice fringes. Ordered straight channels with a spacing of 1.65 nm were observed. The 1.65 nm channel is closed to the pore size of simulated EB-COF:Br structure (1.7 nm). After a restacking process, the nanosheets can be assembled in an integrated membrane. The SEM images reveal that EB-COF:Br membrane is continuous and free of defects on the surface (Fig. 2b), which is critical for efficient separation. The cross-sectional SEM view of EB-COF:Br membrane show a stacked structure similar with laminar GOMs (Fig. 2c).[14,55]

The X-ray diffraction (XRD) was performed to confirm the structure of EB-COF:Br membrane. The XRD of the membrane shows two main peaks which were assigned to the 100 and 001 planes, respectively. As shown in Fig. 2j, the observed XRD matches well with the simulated XRD pattern of the reversed slipped AA-stacking model.[56] We can see clearly that the first peak in the XRD corresponds to the 100 plane which appears at 3.3 Å. And the peak at 27° in the XRD pattern is assigned to the 001 plane that corresponds to the π–π stacking of EB-COF:Br layers. We notice that the peak at 27° is broad and blunt, which is due to the reversed slipped AA-stacking model and the defects in the π–π stacking between successive 2D COF layers.[40,56] Subsequently, structural resolution based on X-ray

View Article Online
DOI: 10.1039/C8TA04178D

diffraction pattern in conjunction with simulated structure indicates that the as-synthesized EB-COF:Br is a typical 2D layered hexagonal network (Fig. 2f, h and Fig. S3, ESI†).[56]

In order to investigate the porosity and pore size of EB-COF:Br membrane, the nitrogen adsorption-desorption experiment of the membrane were performed at 77 K. As shown in Fig. 2i, a sharp increase was observed in gas uptake at low pressure, which means that these are micropores in the membrane. The surface area calculated on the basis of the Brunauer–Emmett–Teller (BET) model is 554 m^2 g^{-1} for EB-COF:Br. We also observe hysteresis curve in desorption, which may be caused by the stack of EB-COF:Br nanosheets. Because it is very difficult to ensure every piece of nanosheets are completely tiled during the process of layer-by-layer restacking. A fraction of nanosheets may be folded or crimped, which will result in interstices between the nanosheets within the membrane (shown in Fig. 2c). The pore size distribution of EB-COF:Br membrane was evaluated by the nonlocal density functional theory method based on the model N_2 at 77 K on carbon. EB-COF:Br exhibits mainly pore size at 16.8 Å (Fig. S4, ESI†). The above results support that EB-COF:Br membrane is porous 2D crystallized COFs membrane with uniform 1D channels.

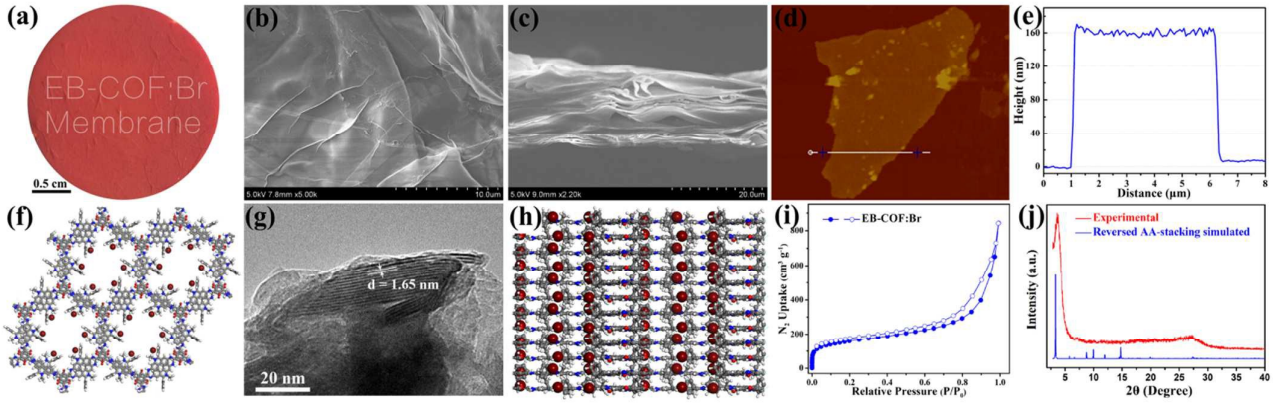

Fig. 2 Characterization of EB-COF:Br nanosheets and EB-COF:Br membrane: (a) Photograph of EB-COF:Br membrane; (b) Surface SEM image of EB-COF:Br membrane; (c) Cross-sectional SEM image fo EB-COF:Br membrane; (d) and (e) AFM images of EB-COF:Br nanosheet showing the surface roughness and thickness recorded on the top of a silicon wafer, respectively; (f) Schematic monolayer extended structure of EB-COF:Br; (g) TEM image of the of EB-COF:Br nanosheets; (h) Side view of the reversed slipped AA-stacking mode structure of EB-COF:Br; (i) Nitrogen sorption isotherm for EB-COF:Br; (j) XRD pattern of EB-COF:Br.

Considering EB-COF:Br membrane has nanosize channels and positive charges on pore walls, which can be utilized for selective sieving for molecules/ions. Initially, the molecular weight cut-off (MWCO) analysis was performed from the rejection of polyethylene glycol (PEG) with different average molecular weights (200, 400, 600, 800, 1000 and 1500 Da). The results show that the EB-COF:Br membrane has 90% rejection of PEG at 882 Da (Fig. 3a). According to the result of MWCO analysis, we can conclude that the porosity of EB-COF:Br membrane is within the nanofltration range. Further, we investigated the permeability of EB-COF:Br membrane to pure solvent. Exhilaratingly, EB-COF:Br membrane exhibits excellent permeance towards protic solvent, including deionized water (546 L m^{-2} h^{-1} bar^{-1}), methanol (1272 L m^{-2} h^{-1} bar^{-1}), ethanol (564 L m^{-2} h^{-1} bar^{-1}), n-propanol (477 L m^{-2} h^{-1} bar^{-1}), n-butanol (378 L m^{-2} h^{-1} bar^{-1}), n-pentanol (248 L m^{-2} h^{-1} bar^{-1}) and n-hexanol (166 L m-2 h-1 bar^{-1}). Meanwhile, the permeability is decreased along with the increasing molecular size of the permeant solvents (Fig. 3b and Table S1, ESI†). To our surprise, the membrane shows higher permeance towards organic aprotic solvents, such as acetone (2640 L m^{-2} h^{-1} bar^{-1}), followed by acetonitrile (2095 L m^{-2} h^{-1} bar^{-1}), tetrahydrofuran (1532 L m^{-2} h^{-1} bar^{-1}), 1,4-dioxane (973 L m^{-2} h^{-1} bar^{-1}) and N,N′-dimethylacetamide (565 L m^{-2} h^{-1} bar^{-1}) (Fig. 3c and Table S2, ESI†). The high permeance of organic aprotic solvents can be attributed to the weak dipole interaction between these aprotic solvents and charged interface aligned in channel in EB-COF:Br membrane. It is worth to mentioning that the solvent permeability of EB-COF:Br membrane is much higher than those of GOMs and other reported nanofltration membranes (See Table S3 for detailed comparisons, ESI†).[8,19,57-59] Further, we also evaluate the impact of membrane thickness to the permeability of pure solvent. The filtration experiment for deionized water is conducted using several membranes with different thickness (146 μm, 195 μm, 241 μm, respectively). As shown in Fig. 3b inset and Table S4 (ESI†), the permeance value of deionized water decreases as the increase of membrane thickness in turn.

Graphene-oxide membranes (GOMs) with interlayer space between GO flakes have been reported to be potential applied in small molecules separation and desalination. However, severe reduction of water permeability was observed in GOMs under pressure-driven permeation test due to the compaction of their loosely packed microstructure. The water flux could drop continuously after more than ten hours as a result of the efficient transport channels were reduced over time.[60,61] One advantage of 2D COF membrane is that they have straight channel along with the solvent transport path (Fig. 1b). We make a comparison of water permeation performance between the EB-COF:Br membrane and GOMs. As shown in Fig. 3d and Fig. S5 and S6 (ESI†), the water permeability of GOMs is 2.5 L m^{-2} h^{-1} bar^{-1} after 30 hours test (Fig. 3d inset, Fig. S5,

View Article Online
DOI: 10.1039/C8TA04178D

ESI†). Although the water permeability of EB-COF:Br membrane is also drastically reduce in the beginning of the permeation test, the steady state water flux of EB-COF:Br membrane is 48 L m^{-2} h^{-1} bar^{-1} after 30 hours continuous testing (Fig. S6, ESI†). This water flux is about 20 times higher than the permeability of GOMs.

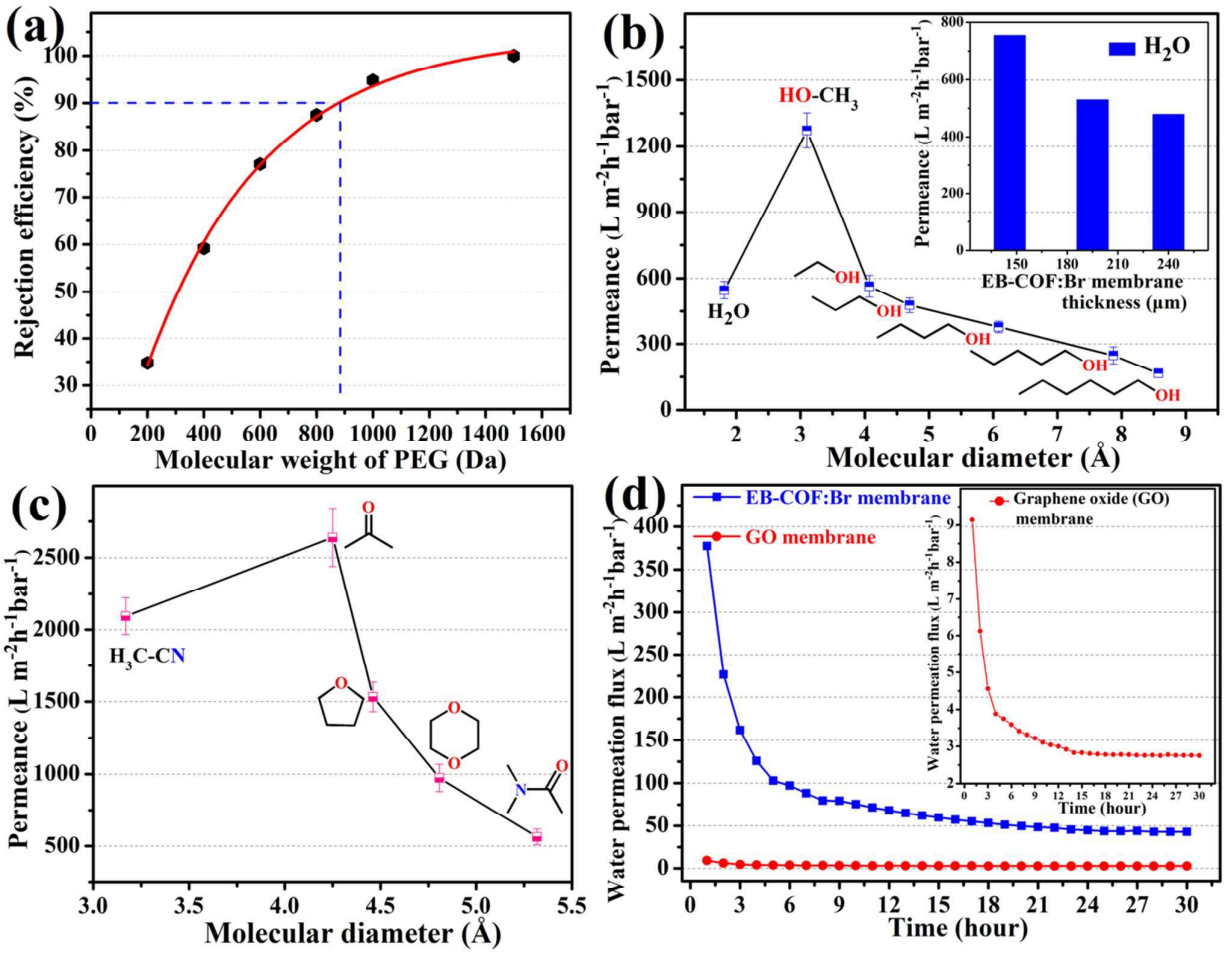

Fig. 3 (a) Molecular-weight cut-off (MWCO) curve showing that the EB-COF:Br membrane has 90% rejection of PEG at 882 Da; (b) Pure solvent permeance versus molecular diameter of different protic (water, methanol, ethanol, n-propanol, n-butanol, 1-Pentanol, n-Hexyl alcohol) and (c) aprotic (acetonitrile, acetone, tetrahydrofuran, 1,4-dioxane, N,N-Dimethylacetamide) solvents; (d) Water permeation flux of EB-COF:Br membrane and GO membrane as a function of time. The membranes were prepared using filtration with thickness about 308 μm for the EB-COF:Br membrane and 3.6 μm for the GO membrane.

The significant advantages of high flux and outstanding chemical stability of EB-COF:Br membrane motivate us to further investigate the rejection performance toward a series of pollutants with environmental and industrial concern. We choose several water-soluble target dyes molecules/ions with different properties of charge, including anionic dyes: Methyl Orange (MO), Fluorescein Sodium salt (FSs) and Potassium Permanganate (PP); Neutral dyes: Nile Red (NR), Calcein (CA) and p-Nitroaniline (NA) and cationic dyes: Rhodamine B (RB), Methylene Blue (MB) and N,N-Dimethyl-p-phenylenediamin dihydrochloride (DMPD). Most of these dyes are mutagenic and carcinogenic in nature, which can cause serious health problems. The sizes of these molecules are assumed by a long-axis dimension of an ellipsoid, as shown in Fig. S7 (ESI†). Their corresponding chemical structures and properties are shown in Fig. 4 and Table S5 (ESI†).

View Article Online
DOI: 10.1039/C8TA04178D

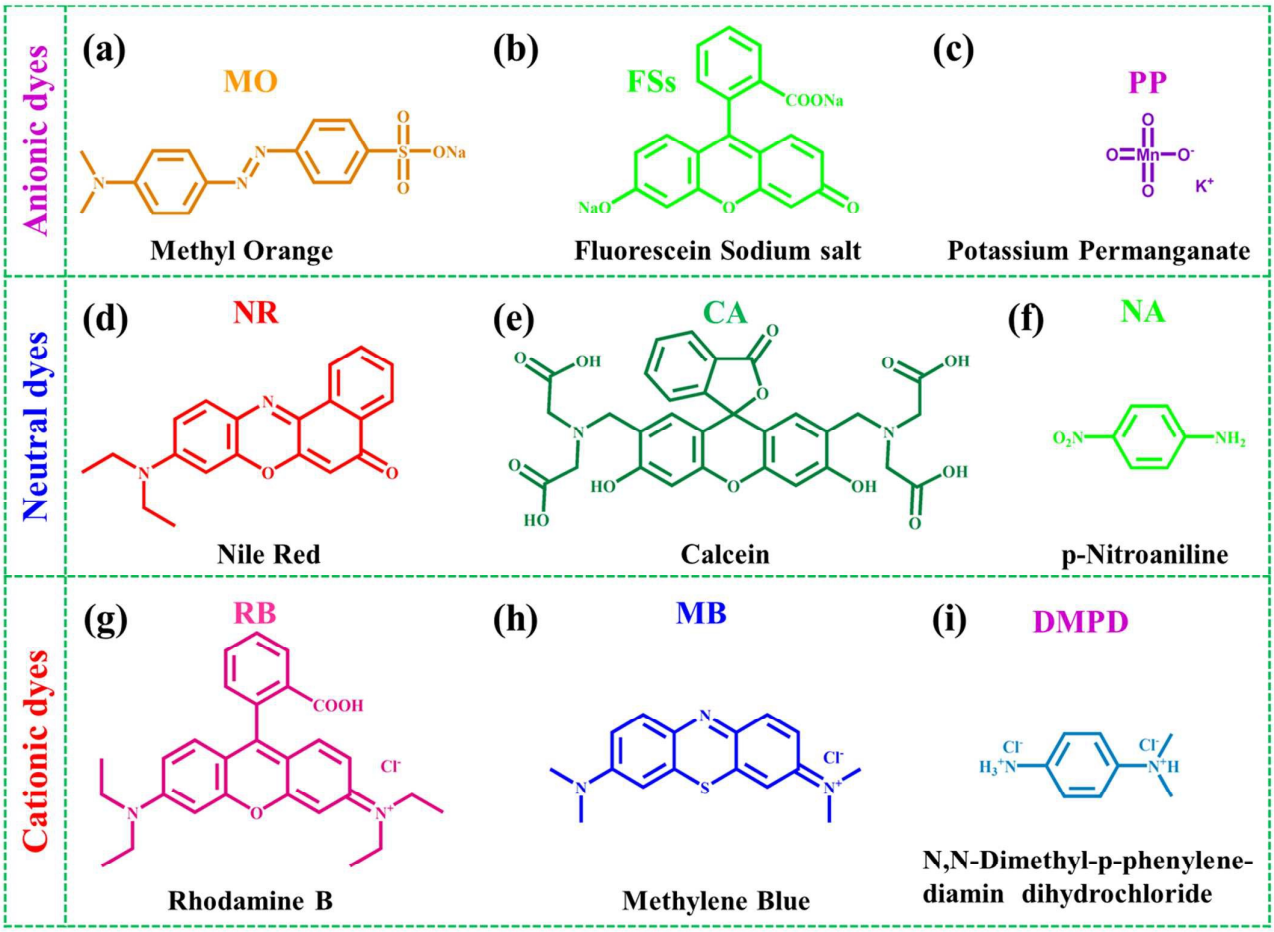

Fig. 4 Chemical structures of dye molecules/ions. (a) MO (methyl orange); (b) FSs (fluorescein sodium salt); (c) PP (potassium permanganate); (d) NR (nile red); (e) CA (calcein); (f) NA (p-nitroaniline); (g) RB (rhodamine B); (h) MB (methylene blue) and (i) DMPD (n,n-dimethyl-p-phenylenediamin dihydrochloride).

We conducted a series of filtration experiments with solutions of dye molecules and ions through EB-COF:Br membrane to verify its rejection performance. The rejection ability of the membrane toward different target dyes was evaluated by monitoring the ultraviolet absorbance intensity of filtrates. As shown in Fig. 5, for anionic dyes (MO, FS and PP), the intensity of absorption spectra of different anionic dyes displays a sharp decrease, as observed in Fig. 5a-c. The characteristics absorption bands of MO, FSs and PP are completely disappeared after filtration through EB-COF:Br membrane. For the three neutral dyes, they present a smaller decline in the intensity of characteristics absorption spectra, especially for NR and NA (Fig. 5d-f). For cationic dyes (RB, MB and DMPD), the characteristic absorption intensity of these dyes is also decreased very significantly (Fig. 5g-i), however, the decreasing amplitude is less than that of the anionic dyes. A more intuitive evidence of the high selective sieving performance of EB-COF:Br membrane is also shown in the Fig. 5, we can observe clearly the color change of different dye solutions before sieving and after sieving via naked eyes under visible light. Remarkably, for anionic dyes, several colorless filtrates are obtained after the EB-COF:Br membrane filtration (Fig. 5j(a-c)). However, other filtrates, from neutral dyes (NR, CA, NA) (Fig. 5k(d-f)) and cationic dyes (RB, MB, DMPD) (Fig. 5l(g-i)) solutions, still retain partial color, which indicates that some dye molecules/ions have permeated the membrane.

View Article Online
DOI: 10.1039/C8TA04178D

Journal of Materials Chemistry A

ARTICLE

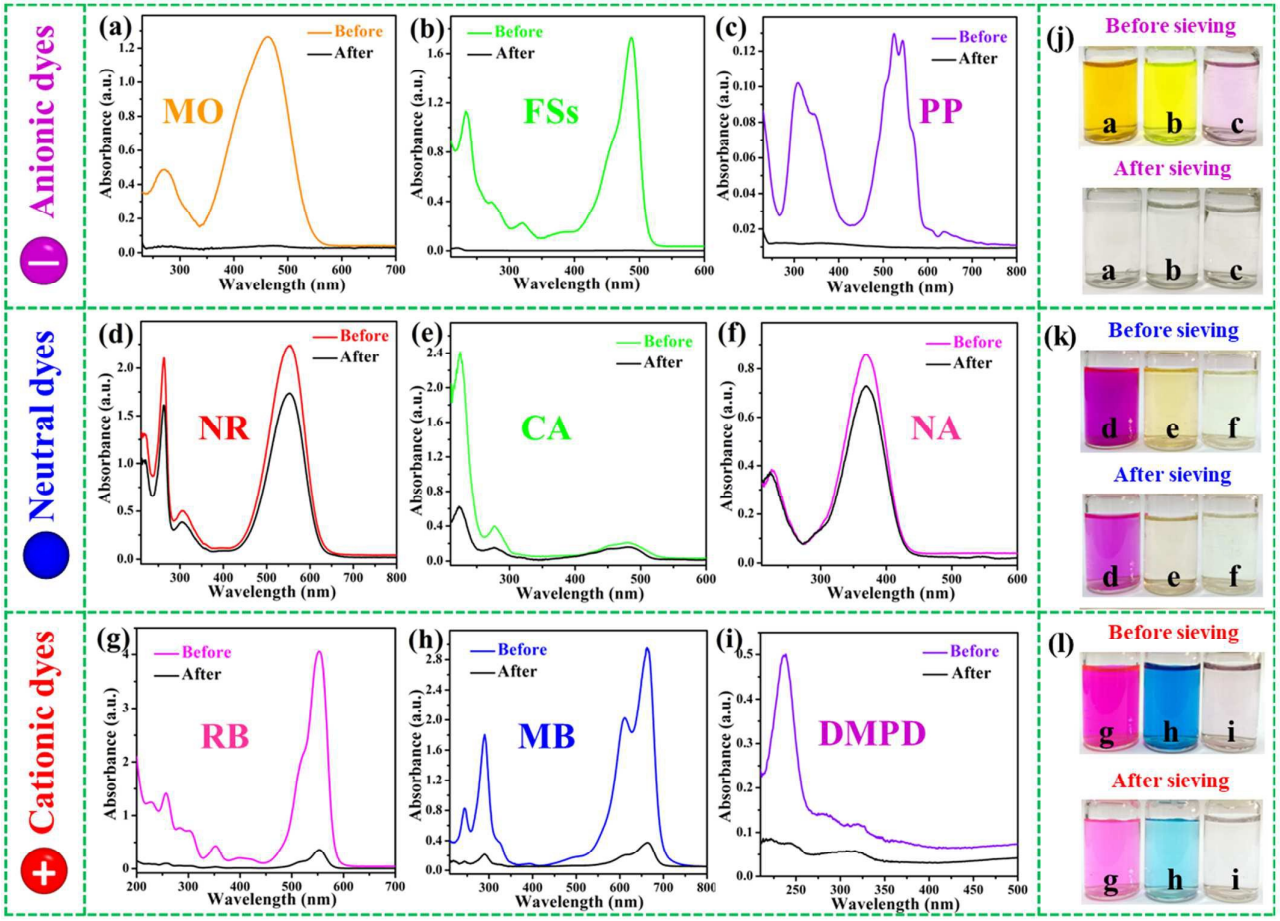

Fig. 5 Charge- and size-selective sieving experiments. (a-i) UV-vis absorption spectra of different dye solutions of (a) MO (methyl orange), (b) FSs (fluorescein sodium salt), (c) PP (potassium permanganate), (d) NR (nile red), (e) CA (calcein), (f) NA (p-nitroaniline), (g) RB (rhodamine B), (h) MB (methylene blue) and (i) DMPD (n, n-dimethyl-p-phenylenediamin dihydrochloride) before sieving and after sieving through EB-COF:Br membrane, respectively. Photographs of different dye solutions color change of before and after sieving are shown in (j), (k), (l), respectively.

In order to more accurately determine the rejection efficiency of EB-COF:Br membrane for different target dyes. A qualitative calculation in terms of Beer-Lambert law is performed. The result shows that the membrane can reject anionic dyes MO, FSs and PP upto 99.6%, 99.2% and 98.1%, respectively. The rejection values of cationic dyes RB, MB and DMPD are 91.2%, 87.2% and 84.9%, respectively. Whereas for neutral dyes of CA, NR and NA, the rejection values are 74.4%, 22.3% and 15.7%, respectively (Fig. 6). The interception efficiency of this 2D cationic membrane for neutral dyes is positive correlation with the molecular size. The rejection efficiency of EB-COF:Br membrane for charged dyes can compete with other high performance membranes. (Table S6, ESI†).

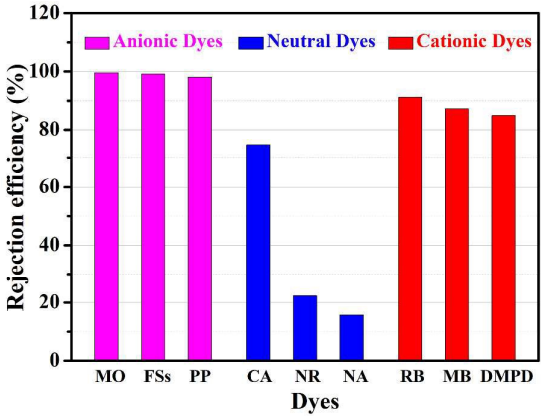

Fig. 6 The rejection efficiency of EB-COF:Br membrane for different dyes.

View Article Online
DOI: 10.1039/C8TA04178D

The above experimental results confirm EB-COF:Br membrane with excellent selective sieving performance for different dye molecules/ions, which is mainly attributed to the following reasons: primarily, plenty of positively charged sites are distributed on the pore walls of EB-COF:Br membrane, which endows the membrane with cationic nature. Moreover, EB-COF:Br has the reversed slipped AA-stacking structure with 16.8 Å pore size. Such spatial alignment vastly enhances the accessibility of cationic sites for guest molecules/ions. Additionally, molecular rejection for the COF membrane not only involves charge-driven separation, but also includes a physical size sieving effect. Based on the structural property of EB-COF:Br membrane, its selective molecular/ionic sieving performance can be explained as follows.

For anionic dyes sieving: in the beginning, the negatively charged molecules can replace the counter-ions Br^{-1} to fit in the channels. Owing to the strong electrostatic interaction between the positively charged pore walls of membrane and anionic dye molecules,[46] the dye molecules will be immobilized into the pores of membrane, preventing them from being moved down along the channels. Moreover, duo to the size limitation of nanoscale channels, only one dye molecule enters EB-COF:Br channel each time. So the subsequent molecule can not across the membrane. Although the channels of EB-COF:Br membrane are blocked by early entered dye molecules, there's still enough space for solvent molecules to pass through the membrane. So the excellent anionic molecules rejection of the membrane is double-controlled by the electrostatic interaction and the limitation of pore size.

In comparison, the rejection values of cationic dyes are lower than those of anionic dyes. Because of there is strong electrostatic repulsion interaction between positive charged pore surface and cationic dye molecules, it will hinder the molecules entered into the pore channels of EB-COF:Br membrane. In spite of this, small cationic dye molecules such as DMPD still be able to diffuse into the channels slowly. Due to there is repulsive force in the positive charged pore, the cationic dye molecules can not be fixed in the channels and they will cross the membrane. So the discrepancy of separation efficiency between cationic dye molecules is mainly originated from their molecular sizes (Fig. S7g-i, ESI†).

As for neutral dye molecules, the electrostatic interaction between dye and EB-COF:Br is very weak. Hence, the rejection efficiency is mainly attributed to molecular size sieving effect. As showed in Fig. 6, the rejection values for neutral dye are in good agreement with their molecular size: NA < NR < CA (Fig. 5d-f, Fig. 6 and Fig. S7d-f, ESI†).

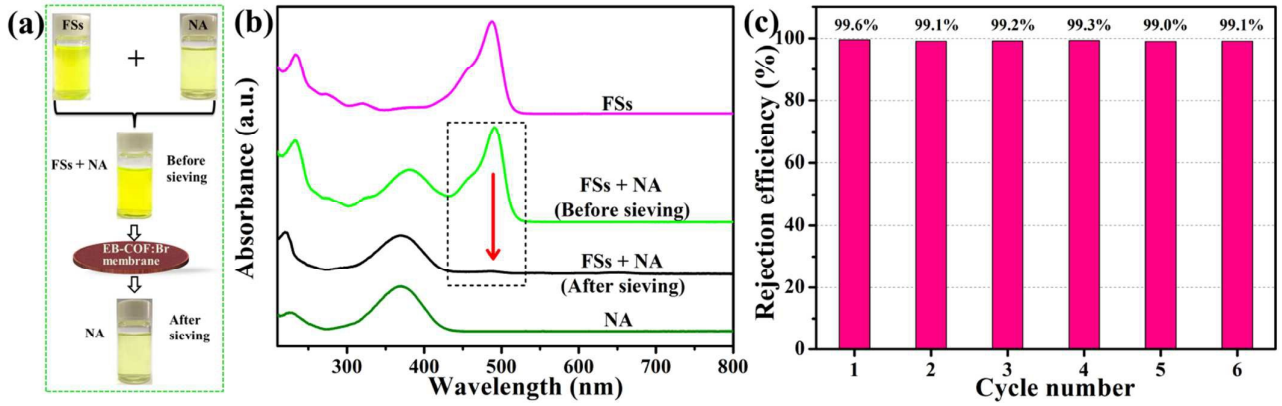

Fig. 7 (a) Photograph schematic of the selective molecular separation of nitroaniline (NA) from a mixture of NA and Fluorescein Sodium salt (FSs); (b) UV-vis absorption spectra of selective sieving of NA from the mixed solution of NA and FSs; (c) Cycle performance of MO rejection through EB-COF:Br membrane.

To evaluate the mixed dyes solution separation ability of the membrane, a mixed solution of FSs (Fluorescein Sodium salt) and NA (Nitroaniline) is filtered via EB-COF:Br membrane. As shown in Fig. 7, a greenish yellow mixed solution [derived from yellow (FSs) and reseda (NA)] is filtered through EB-COF:Br membrane, resulting in a light yellow NA filtrate (Fig. 7a). This result is further confirmed by comparing the UV-vis absorption spectra of mixed solution before and after separation, respectively. The concentration of FSs in the filtrate is decreased by 98%, whereas NA does not show any notable changes (Fig. 7b), which consequently confirms that FSs and NA can be effectively separated. In addition, another mixed dyes solution (including anionic, neutral and cationic dyes) had also been filtered via EB-COF:Br membrane. As shown in Fig. S8 and S9 (ESI†), the absorbance spectrum of solution before- and after-filtration further demonstrated EB-COF:Br membrane could thoroughly intercept the anionic dye molecules, which manifesting its potential application towards complex wastewater treatment in textile/dye industries.

As a promising separation membrane, the recyclability is very important. Here, a cycling study of EB-COF:Br membrane for MO interception is carried out. The result demonstrates that the cationic nanochannels of EB-COF:Br membrane can be easily rinsed thoroughly and regenerated by treating the membrane with aqueous NaBr solution (2.0 mol L^{-1}). As shown in Fig. 7c and Fig. S10 (ESI†), the rejection efficiency of the recycled EB-COF:Br membrane for MO is above 99.1% even after six cycles. Further, the time course of rejection efficiency of EB-COF:Br membrane for anionic dye (MO) was also performed to investigate the durability of the membrane. As

View Article Online
DOI: 10.1039/C8TA04178D

seen in Fig. S11 (ESI†), the membrane still exhibits >99% rejection efficiency for MO after 10-hours continuous operation. All the above results indicate that the cationic COFs membrane combines selectivity, efficiency and recyclability in rejection anionic dyes, which manifesting its potential application towards wastewater treatment in textile/dye industries and environmental protection.

Conclusions

In summary, a 2D cationic crystallized COFs membrane, namely EB-COF:Br membrane, was fabricated by a facile bottom-up interfacial crystallization approach and layer-by-layer restacking process. We demonstrated that the 2D EB-COF:Br offered an excellent scaffold for creating ionic interfaces in pore walls along the channels in the membrane. The resulting EB-COF:Br membrane exhibited remarkable selective molecular sieving performance based on their different sizes and charges. Given the unique structure of EB-COF:Br membrane, physical size sieving and electrostatic interactions are considered as the vital role in the process of separation. The reported cationic 2D COFs membrane exhibits extraordinary separation property with high solvent permeability. With the ultrafast solvent transport and selective molecular sieving property, ionic COFs membrane can be presented as an interesting platform for separation and filtration technologies.

Conflicts of interest

The authors declare no competing financial interests.

Acknowledgements

The authors gratefully thank the financial supports of the NSFC (Grant Nos. 21773223, 21673218, 51572256, 21501166) and the Science and Technology Developing Project of Jilin Province (Grant No. 20170520135JH, 20180101177JC, 20180101176JC). The authors also thank the Open Funds of the State Key Laboratory of Rare Earth Resource Utilization and State Key Laboratory of Inorganic Synthesis and Preparative Chemistry, Jilin University.

Notes and references

1 J. W. Colson, W. R. Dichtel, *Nat. Chem.*, 2013, **5**, 453-465.
2 Y. Ying, Y. Yang, W. Ying, X. Peng, *Nanotechnology*, 2016, **27**, 332001.
3 L. S. Wan, J. W. Li, B. B. Ke, Z. K. Xu, *J. Am. Chem. Soc.*, 2012, **134**, 95-98.
4 P. Sun, K. Wang, H. Zhu, *Adv. Mater.*, 2016, **28**, 2287-2310.
5 Q. Wen, D. Yan, F. Liu, M. Wang, Y. Ling, P. Wang, P. Kluth, D. Schauries, C. Trautmann, P. Apel, W. Guo, G. Xiao, J. Liu, J. Xue, Y. Wang, *Adv. Funct. Mater.*, 2016, **26**, 5796-5803.
6 A. Lee, J. W. Elam, S. B. Darling, *Environ. Sci.: Water Res. Technol.*, 2016, **2**, 17-42.
7 R. K. Joshi, P. Carbone, F. C. Wang, V. G. Kravets, Y. Su, I. V. Grigorieva, H. A. Wu, A. K. Geim, R. R. Nair, *Science*, 2014, **343**, 752-754.
8 Q. Yang, Y. Su, C. Chi, C. T. Cherian, K. Huang, V. G. Kravets, F. C. Wang, J. C. Zhang, A. Pratt, A. N. Grigorenko, F. Guinea, A. K. Geim, R. R. Nair, *Nat. Mater.*, 2017, **16**, 1198-1202.
9 H. M. Hegab, L. Zou, *J. Membr. Sci.*, 2015, **484**, 95-106.
10 10 J. R. Werber, C. O. Osuji, M. Elimelech, *Nat. Rev. Mater.*, 2016, **1**, 16018.
11 D. Cohen-Tanugi, J. C. Grossman, *Nano Lett.*, 2012, **12**, 3602-3608.
12 F. X. Xiao, M. Pagliaro, Y. J. Xu, B. Liu, *Chem. Soc. Rev.*, 2016, **45**, 3088-3121.
13 H. Huang, Z. Song, N. Wei, L. Shi, Y. Mao, Y. Ying, L. Sun, Z. Xu, X. Peng, *Nat. commun.*, 2013, **4**, 2979.
14 K. Raidongia, J. Huang, *J. Am. Chem. Soc.*, 2012, **134**, 16528-16531.
15 H. Li, Z. Song, X. Zhang, Y. Huang, S. Li, Y. Mao, H. J. Ploehn, Y. Bao, M. Yu, *Science*, 2013, **342**, 95-98.
16 P. R. Kidambi, M. S. H. Boutilier, L. Wang, D. Jang, J. Kim, R. Karnik, *Adv. Mater.*, 2017, **29**, 1605896.
17 G. Liu, W. Jin, N. Xu, *Chem. Soc. Rev.*, 2015, **44**, 5016-5030.
18 K. Celebi, J. Buchheim, R. M. Wyss, A. Droudian, P. Gasser, I. Shorubalko, J. I. Kye, C. Lee, H. G. Park, *Science*, 2014, **344**, 289-292.
19 Y. Han, Z. Xu, C. Gao, *Adv. Funct. Mater.*, 2013, **23**, 3693-3700.
20 C. Cheng, G. Jiang, C. J. Garvey, Y. Wang, G. P. Simon, J. Z. Liu, D. Li, *Sci. Adv.*, 2016, **2** ,1501272.
21 L. Chen, G. Shi, J. Shen, B. Peng, B. Zhang, Y. Wang, F. Bian, J. Wang, D. Li, Z. Qian, G. Xu, G. Liu, J. Zeng, L. Zhang. Y. Yang, G. Zhou, M. Wu, W. Jin, J. Li, H. Fang, *Nature*, 2017, **550**, 380-383.
22 A. R. Koltonow, J. Huang, *Science*, 2016, **351**, 1395-1396.
23 S. Wang, Y. Xie, G. He, Q. Xin, J. Zhang, L. Yang, Y. Li, H. Wu, Y. Zhang, M. D. Guiver, Z. Jiang, *Angew. Chem., Int. Ed.*, 2017, **56**, 14246-14251.
24 U. Díaz, A. Corma, *Coord. Chem. Rev.*, 2016, **311**, 85-124.
25 R. P. Bisbey, W. R. Dichtel, *ACS Cent. Sci.*, 2017, **3**, 533-543.
26 C. S. Diercks, O. M. Yaghi, *Science*, 2017, **355**, 923-931.
27 X. Zhuang, Y. Mai, D. Wu, F. Zhang, X. Feng, *Adv. Mater.*, 2015, **27**, 403-427.
28 N. Huang, X. Chen, R. Krishna, D. Jiang, *Angew. Chem., Int. Ed.*, 2015, **54**, 2986-2990.
29 J. L. Segura, M. J. Mancheno, F. Zamora, *Chem. Soc. Rev.*, 2016, **45**, 5635-5671.
30 P. J. Waller, F. Gandara, O. M. Yaghi, *Acc. Chem. Res.*, 2015, **48**, 3053-3063.
31 S. Kandambeth, B. P. Biswal, H. D. Chaudhari, K. C. Rout, H. S. Kunjattu, S. Mitra, S. Karak, A. Das, R. Mukherjee, U. K. Kharul, R. Banerjee, *Adv. Mater.*, 2017, **29**, 1603945.
32 S. Y. Ding, W. Wang, *Chem. Soc. Rev.*, 2013, **42**, 548-568.
33 S. Kandambeth, A. Mallick, B. Lukose, M. V. Mane, T. Heine, R. Banerjee, *J. Am. Chem. Soc.*, 2012, **134**, 19524-19527.
34 J. W. Colson, A. R. Woll, A. Mukherjee, M. P. Levendorf, E. L. Spitler, V. B. Shields, M. G. Spencer, J. Park, W. R. Dichtel, *Science*, 2011, **332**, 228-231.
35 S. Chandra, S. Kandambeth, B. P. Biswal, B. Lukose, S. M. Kunjir, M. Chaudhary, R. Babarao, T. Heine, R. Banerjee, *J. Am. Chem. Soc.*, 2013, **135**, 17853-17861.
36 J. Zhang, Y. Chen, X. Wang, *Energ. Environ.Sci.*, 2015, **8**, 3092-3108.

View Article Online
DOI: 10.1039/C8TA04178D

37 D. N. Bunck, W. R. Dichtel, *J. Am. Chem. Soc.*, **2013**, **135**, 14952-14955.
38 S. Wang, Q. Wang, P. Shao, Y. Han, X. Gao, L. Ma, S. Yuan, X. Ma, J. Zhou, X. Feng, B. Wang, *J. Am. Chem. Soc.*, 2017, **139**, 4258-4261.
39 G. Das, B. P. Biswal, S. Kandambeth, V. Venkatesh, G. Kaur, M. Addicoat, T. Heine, S. Verma, R. Banerjee, *Chem. Sci.*, 2015, **6**, 3931-3939.
40 Z. Kang, Y. Peng, Y. Qian, D. Yuan, M. A. Addicoat, T. Heine, Z. Hu, L. Tee, Z. Guo, D. Zhao, *Chem. Mater.*, 2016, **28**, 1277-1285.
41 S. Mitra, S. Kandambeth, B. P. Biswal, M. A. Khayum, C. K. Choudhury, M. Mehta, G. Kaur, S. Banerjee, A. Prabhune, S. Verma, S. Roy, U. K. Kharul, R. Banerjee, *J. Am. Chem. Soc.*, 2016, **138**, 2823-2828.
42 M. A. Khayum, S. Kandambeth, S. Mitra, S. B. Nair, A. Das, S. S. Nagane, R. Mukherjee, R. Banerjee, *Angew. Chem., Int. Ed.*, 2016, **55**, 15604-15608.
43 X. H. Liu, C. Z. Guan, D. Wang, L. J. Wan, *Adv. Mater.*, 2014, **26**, 6912-6920.
44 K. Dey, M. Pal, K. C. Rout, H. S. Kunjattu, A. Das, R. Mukherjee, U. K. Kharul, R. Banerjee, *J. Am. Chem. Soc.*, 2017, **139**, 13083-13091.
45 D. Xu, J. Guo, F. Yan, *Prog. Polym. Sci.*, 2018, **79**, 121-143.
46 N. Huang, P. Wang, M. A. Addicoat, T. Heine, D. Jiang, *Angew. Chem., Int. Ed.*, 2017, **56**, 4982-4986.
47 C. Yan, C. Lv, Y. Zhu, G. Chen, J. Sun, G. Yu, *Adv. Mater.*, 2017, **29**, 1703909.
48 X. Lin, Q. Yang, L. Ding, B. Su, *ACS Nano*, 2015, **9**, 11266-11277.
49 Y. Ying, D. Liu, J. Ma, M. Tong, W. Zhang, H. Huang, Q. Yang, C. Zhong, *J. Mater. Chem. A*, 2016, **4**, 13444-13449.
50 J. J. Shao, K. Raidongia, A. R. Koltonow, J. Huang, *Nat. commun.*, 2015, **6**, 7602.
51 R. Sakamoto, K. Hoshiko, Q. Liu, T. Yagi, T. Nagayama, S. Kusaka, M. Tsuchiya, Y. Kitagawa, W. Y. Wong, H. Nishihara, *Nat. commun.*, 2015, **6**, 6713.
52 W. Dai, F. Shao, J. Szczerbinski, R. McCaffrey, R. Zenobi, Y. Jin, A. D. Schluter, W. Zhang, *Angew. Chem., Int. Ed.*, 2016, **55**, 213-217.
53 R. Dong, M. Pfeffermann, H. Liang, Z. Zheng, X. Zhu, J. Zhang, X. Feng, *Angew. Chem., Int. Ed.*, 2015, **54**, 12058-12063.
54 B. P. Biswal, S. Chandra, S. Kandambeth, B. Lukose, T. Heine, R. Banerjee, *J. Am. Chem. Soc.*, 2013, **135**, 5328-5331.
55 R. R. Nair, H. A. Wu, P. N. Jayaram, I. V. Grigorieva, A. K. Geim, *Science*, 2012, **335**, 442.
56 H. Ma, B. Liu, B. Li, L. Zhang, Y. G. Li, H. Q. Tan, H. Y. Zang, G. Zhu, *J. Am. Chem. Soc.*, 2016, **138**, 5897-5903.
57 S. Y. Yang, I. Ryu, H. Y. Kim, J. K. Kim, S. K. Jang, T. P. Russell, *Adv. Mater.*, 2006, **18**, 709-712.
58 J. E. Gu, S. Lee, C. M. Stafford, J. S. Lee, W. Choi, B. Y. Kim, K. Y. Baek, E. P. Chan, J. Y. Chung, J. Bang, J. H. Lee, *Adv. Mater.*, 2013, **25**, 4778-4782.
59 S. Karan, Z. Jiang, A. G. Livingston, *Science*, 2015, **348**, 1347-1351.
60 J. Y. Chong, B. Wang, K. Li, *Chem. Commun.*, 2018, **54**, 2554-2557.
61 J. Y. Chong, B. Wang, C. Mattevi, K. Li, *J. Membr. Sci.*, 2018, **549**, 385-392.

View Article Online
DOI: 10.1039/C8TA04178D

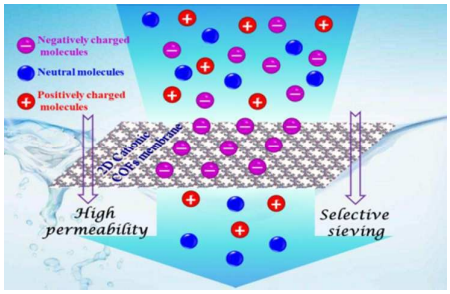

Two-dimensional cationic covalent organic framework membrane with extraordinary separation property and high permeability.